nature nanotechnology

LETTERS

PUBLISHED ONLINE: 20 MARCH 2011 | DOI: 10.1038/NNANO.2011.38

Three-dimensional bicontinuous ultrafast-charge and -discharge bulk battery electrodes

Huigang Zhang, Xindi Yu and Paul V. Braun*

Rapid charge and discharge rates have become an important feature of electrical energy storage devices, but cause dramatic reductions in the energy that can be stored or delivered by most rechargeable batteries (their energy capacity)[1–7]. Supercapacitors do not suffer from this problem, but are restricted to much lower stored energy per mass (energy density) than batteries[8]. A storage technology that combines the rate performance of supercapacitors with the energy density of batteries would significantly advance portable and distributed power technology[2]. Here, we demonstrate very large battery charge and discharge rates with minimal capacity loss by using cathodes made from a self-assembled three-dimensional bicontinuous nanoarchitecture consisting of an electrolytically active material sandwiched between rapid ion and electron transport pathways. Rates of up to 400C and 1,000C for lithium-ion and nickel-metal hydride chemistries, respectively, are achieved (where a 1C rate represents a one-hour complete charge or discharge), enabling fabrication of a lithium-ion battery that can be 90% charged in 2 minutes.

Approaches for enhancing ion and electron transport kinetics in batteries include designing electrode materials with high ion diffusion constants[6,7] and coating the electrolytically active material with a conductive layer, typically carbon[2,3,9]. It is well known that reductions in the characteristic dimensions of the electrolytically active material are more effective in improving battery cycling rates than increases in ion diffusivity D, because the characteristic time constant t for diffusion is proportional to the square of the diffusion length L ($t \approx L^2/D$)[5,8]. By definition, nanoscale electrodes have exceptionally short ion and electron transport lengths[10,11]. However, it has proven difficult to concurrently obtain a high volume fraction of nanostructured electrolytically active material and efficient ion and electron pathways. As discussed by Long and Rolison, the ideal electrode architecture for providing efficient ion and electron transport consists of a three-dimensional interpenetrating network of electron and ion pathways[7,12], and initial strides have been made to fabricate such structures. Copper pillar array[1], nickel network[13–18], stainless steel mesh[19], polymer scaffold[20], and coaxial[21], nanotube[22] and nanofoam[23] carbonaceous interpenetrating structures have been fabricated to serve as conductive pathways in battery cathodes and anodes. However, in these structures, long-range ion diffusion is still required. The macroporous lithium-ion electrodes fabricated by Stein[24–27] and Dunn[28] by means of colloid templating reduce the ion transport length and are particularly promising; however, the relatively low electrical conductivity of the macroporous host significantly limits the rate performance. In general, only modest improvements in rate performance have been observed, because the mesoporous structures primarily address ion and not electron transport. Realization of an electrochemical energy storage system with supercapacitor-like rate performance and battery-like capacity requires the simultaneous minimization of the four primary resistances present during charge and discharge (Fig. 1b): (i) ion transport in the electrolyte[29], (ii) ion transport in the electrode, (iii) electrochemical reactions in the electrode and (iv) electron conduction in the electrode and current collector[1,5,7].

Here, we report a self-assembled bicontinuous bulk electrode concept consisting of an electrolytically active material sandwiched between highly conductive ion and electron transport pathways (Fig. 1a), which, by simultaneously addressing all four resistances, enables ultrafast discharge and charge. This bicontinuous electrode provides (i) an interconnected electrolyte-filled pore network that enables rapid ion transport, (ii) a short solid-phase ion diffusion length minimizing the effect of sluggish solid-state ion transport, (iii) a large electrode surface area and (iv) high electron conductivity in the electrode assembly (Fig. 1b). Two examples, a nickel oxyhydroxide cathode for a nickel metal hydride (NiMH) battery and lithiated MnO_2 for a lithium-ion battery confirm that this electrode design enables ultrafast, supercapacitor-like discharge and charge rate capability while maintaining battery-like storage capacities, despite the fact that these materials have relatively low electron and/or ion conductivities[3] (Supplementary Table 1).

The bicontinuous electrode was fabricated as outlined in Fig. 1c (for details, see Supplementary Information). Self-assembled opal templates were prepared from 1.8 μm polystyrene spheres for the NiMH cathode and 466 nm polystyrene spheres for the lithium-ion cathode. Smaller colloids were used to form the lithium-ion cathode template because of the lower electron and ion conductivity in the electrolytically active phase for the lithium-ion cathode relative to the NiMH cathode, which makes shorter solid-state diffusion lengths desirable. Nickel was then electrodeposited through the templates. Template removal resulted in a nickel inverse opal (~74% porosity) containing very narrow interconnects between the spherical voids, formed by the contact points of the colloidal spheres in the template. If this structure were directly filled with the electrolytically active phase, the narrow interconnects would rapidly close during deposition, preventing conformal deposition of the electrolytically active material into the depths of the structure. The resulting ion pathway would then not be continuous, limiting allowable charge and discharge rates. Electropolishing was used to increase the overall porosity to ~94%, a few percent below the maximum theoretical porosity of 96.4 vol% (Supplementary Fig. 1), and to enlarge the interconnect window size between adjacent pores[30] (Fig. 2a,d). Finally, the electrolytically active material (NiOOH for the NiMH cathode and MnO_2 for the lithium-ion cathode) was electrodeposited into the now highly porous nickel framework (Fig. 2b,e). Pulsed electrodeposition was used to ensure conformal electrodeposition through the complex three-dimensional structure, and anodic deposition was used to achieve good electrical and mechanical contact of the electrodeposited material with the conductive scaffold[31,32]. The MnO_2 was subsequently lithiated in a molten salt

Department of Materials Science and Engineering, Materials Research Laboratory, and Beckman Institute, University of Illinois at Urbana-Champaign, Urbana, Illinois 61801, USA. *e-mail: pbraun@illinois.edu

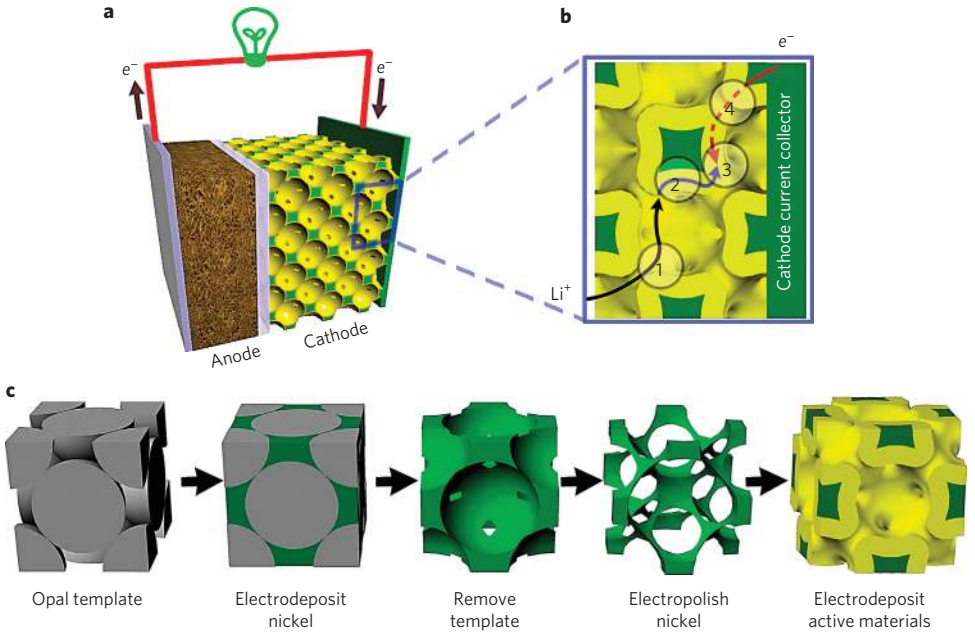

Figure 1 | Bicontinuous battery electrode. a, Schematic of a battery containing a bicontinuous cathode. **b**, Illustration of the four primary resistances in a battery electrode. **c**, Bicontinuous electrode fabrication process. The electrolytically active phase is yellow and the porous metal current collector is green. The electrolyte fills the remaining pores.

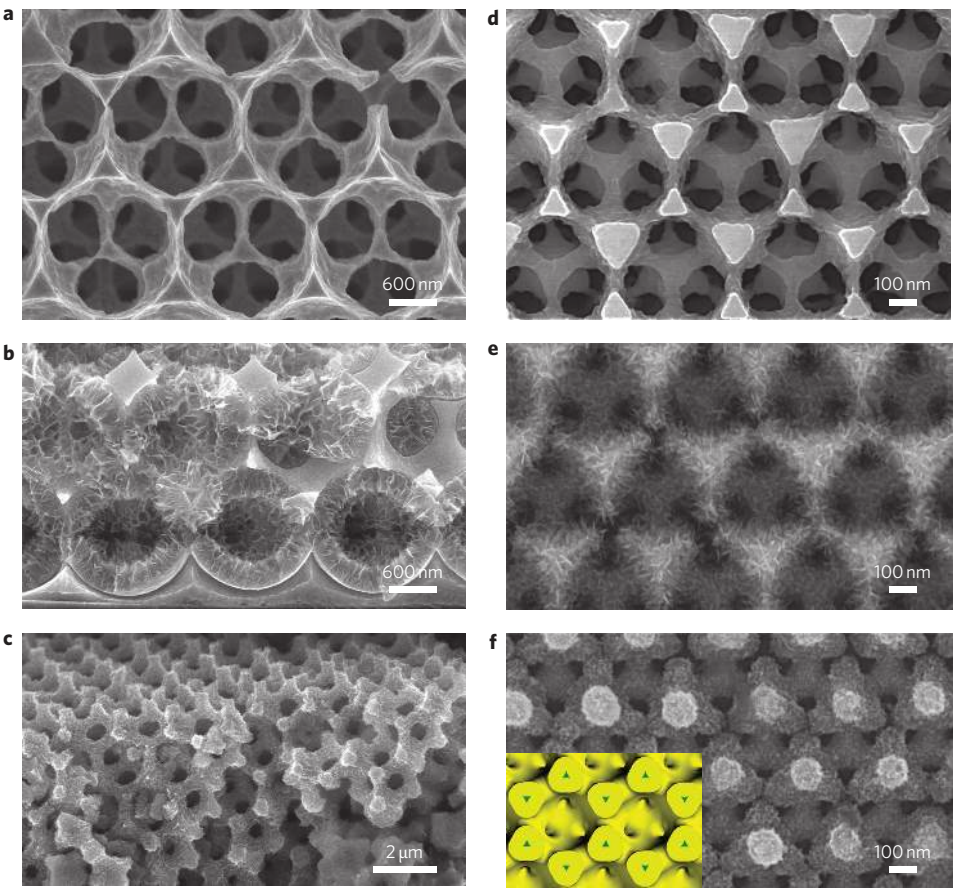

Figure 2 | Bicontinuous electrode microstructure. SEM images of a bicontinuous three-dimensional electrode during each step of preparation. **a**, Nickel inverse opal after electropolishing (1.8 μm colloidal particle template). **b**, Cross-section of NiOOH/nickel composite cathode. **c**, Cross-section of NiOOH/nickel cathode after cycling. **d**, Nickel inverse opal after electropolishing (466 nm colloidal particle template). **e**, MnO_2/nickel composite cathode. **f**, Lithiated MnO_2/nickel composite cathode.

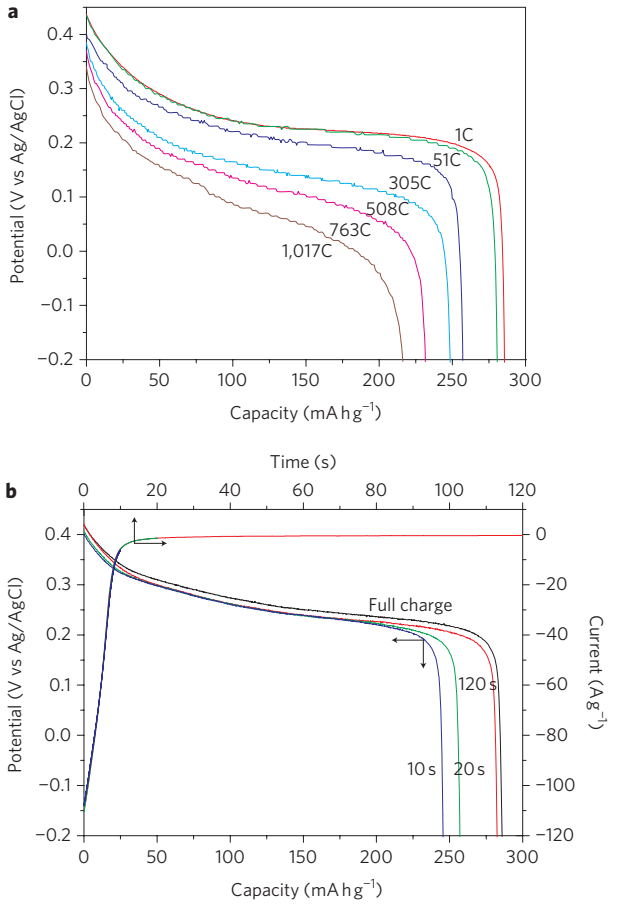

Figure 3 | Ultrafast discharge and charge of the NiOOH electrode. a, Discharge curves of NiOOH/nickel cathode at various C-rates. **b**, Constant potential charge curves (0.45 V versus silver/AgCl) and 6C discharge curves after charging at constant potential for the indicated time. The curve labelled 'full charge' was charged galvanostatically at 1C.

mixture of $LiNO_3$ and LiOH (Fig. 2f). This bicontinuous sandwich architecture, consisting of a thin layer of electrolytically active material between three-dimensionally connected electrolyte and conductive scaffold phases, provides a highly conductive pathway for electrons, a short ion diffusion length in the intercalation compound, and a fast mass transport channel in the liquid electrolyte. The thickness of a typical bicontinuous electrode is ~10 μm and, as described in the Supplementary Information, can also be made much thicker. Characterization of the electrolytically active materials is described in Supplementary Figs 2 and 3. Other potential battery chemistries using our bicontinuous electrode concept are also discussed in the Supplementary Information.

The electrochemical performance of the NiOOH cathode was examined in a three-electrode system using saturated silver/AgCl as the reference and platinum foil as the counter-electrode. Discharge curves at various C-rates are presented in Fig. 3a (the C-rate^{-1} is the time in hours required to fully charge or discharge an electrode or battery; an *n*C-rate indicates that the current chosen will discharge the system in $1/n$ h). At 305C, the NiOOH cathode delivers 90% of its 1C capacity, and when the discharge rate increases to the unprecedented value of 1,017C (291 A g^{-1}), the electrode delivers 75% of its 1C capacity in ~2.7 s. In comparison, commercial NiMH cathodes, which consist of a large-pore-size (~50 μm to 1 mm) nickel foam coated with a thick layer of NiOOH, usually retain ~1–2% of their capacity at C-rates exceeding 35C (ref. 4). The low capacity at high C-rates in a conventional electrode is in part due to sluggish proton diffusion in the active material layer, which strongly depends on the state of charge of the electrode and varies by about three orders of magnitude from 3.4×10^{-8} cm^2 s^{-1} when completely charged to 6.4×10^{-11} cm^2 s^{-1} when completely discharged[33], and the high resistance of the $Ni(OH)_2$ that forms on the relatively conductive NiOOH during discharge: $NiOOH + H_2O + e^- \rightarrow Ni(OH)_2 + OH^-$ (refs 34,35). As a result, in a conventional electrode, high internal resistances are present, even at modest discharge levels. The gravimetric capacity of our NiOOH is 286 mA h g^{-1}, which is close to the theoretical value for a single electron transfer process[35], indicating that deposition of the NiOOH into a bicontinuous architecture does not negatively impact its properties. Constant potential (0.45 V versus silver/AgCl) was applied to examine the charging behaviour of the nickel hydroxide cathode. The results show that the initial charging current is ~110 A g^{-1} (~385C), but decreases rapidly to almost zero in ~20 s (Fig. 3b) as the cathode becomes fully charged. The discharge curves after various charging times (Fig. 3b) show that the electrode is 85% charged after 10 s and 90% charged after 20 s. The capacity delivered after a 120 s charge is 99.0% of the 1C galvanostatic charge. After 100 cycles (6C charge and discharge), the capacity retention of the NiOOH electrode is 95% (Supplementary Fig. 4), and electrode morphology remains unchanged (Fig. 2c).

Similar results were obtained for the bicontinuous lithiated MnO_2 cathode (the thickness of the lithiated MnO_2 layer is ~30 nm) using lithium counter- and reference electrodes and 1 M $LiClO_4$ in a 1:1 by mass mixture of ethylene carbonate and dimethylene carbonate as electrolyte (Fig. 4). The bicontinuous lithiated MnO_2 electrode (Fig. 2f) retains 76% of its capacity when discharged at 185C, and 38% when discharged at 1,114C. If a thicker (~150–200 nm) active layer (Supplementary Fig. 5b) is deposited to increase the electrode energy density, the high rate capacity decreases, but the capacity still remains at 34% at 615C and 60% at 62C (Supplementary Fig. 6). Because thinner layers are required for high-rate discharge in the lithium-ion cathode relative to the NiMH cathode, to shorten the solid-state diffusion length, the colloidal crystal template used for the lithium-ion cathode was constructed from smaller colloidal particles (diameter, 466 nm) rather than the 1.8-μm-diameter polystyrene spheres used for the NiMH cathode. The higher surface area of the smaller sphere system results in a greater energy density for a given thickness of electrolytically active material. The intrinsic properties of the lithiated MnO_2 are as expected. Deposition into a morphologically complex structure does not seem to change its fundamental electrochemical properties. It can be estimated by geometric analysis using measurements from scanning electron microscopy (SEM) images that the electrode in Supplementary Fig. 5b is 67 vol% active materials.

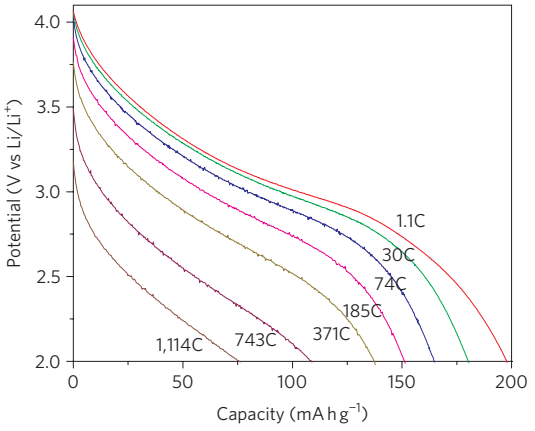

Figure 4 | Ultrafast discharge of the lithiated MnO_2 cathode. The lithiated MnO_2 cathode was discharged at C-rates ranging from 1.1 to 1,114C.

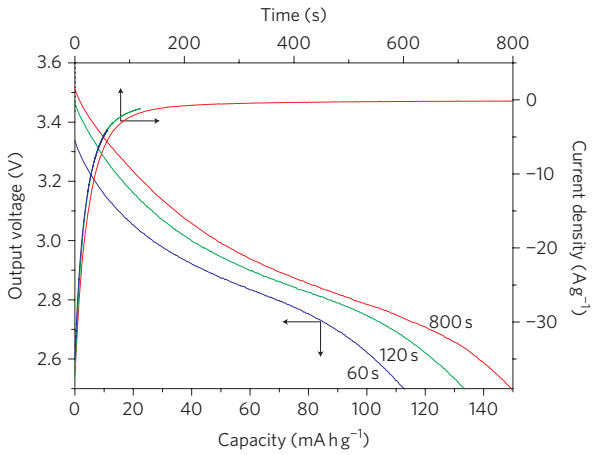

Figure 5 | Lithium-ion battery ultrafast charge behaviour. Potentiostatic charging at 3.6 V for 60 s (blue), 120 s (green) and 800 s (red), and ~3C galvanostatic discharging of the prototype lithium-ion pouch battery after each charging cycle.

Because the volume is the cube of the radius, what seems to be only a thin layer of active material deposited on the shell will occupy a relatively large volume compared with the central void, without closing the central void. This is why the inverse structure has both high power and energy density. Assuming a potential window of 4.2–2.0 V, the gravimetric capacity of the lithiated MnO_2 is 198 mA h g^{-1}, which is similar to previous reports on similarly synthesized lithiated MnO_2 (ref. 36). The fact that the lithium-ion discharge curves do not exhibit a flat stage is a function of the synthetic procedure used to form the lithiated MnO_2 layer[36], and not a result of the bicontinuous electrode architecture. After 50 cycles (3C charge and discharge), the capacity retention of the lithiated MnO_2 electrode is 88% (Supplementary Fig. 7).

A prototype lithium-ion battery was assembled from a bicontinuous lithiated MnO_2 cathode, together with a graphite anode, a separator and 1 M $LiClO_4$ as the electrolyte, and sealed in a moisture barrier bag. The anode capacity was selected to be about ten times greater than that of the cathode so that the anode was not rate-limiting. A constant potential (3.6 V) was applied. The initial charge current was 35 A g^{-1} (~177C) and rapidly decreased to almost zero in 120 s (Fig. 5). The discharge curves in Fig. 5 show that after 60 s the battery is charged to 75% capacity, and after 120 s it is 90% charged relative to a 800 s charge. Charging past 800 s resulted in insignificant increases in capacity.

In conclusion, we have demonstrate a general paradigm for creating high-rate rechargeable batteries through the use of a bicontinuous three-dimensional composite battery electrode design that provides efficient and rapid pathways for ion and electron transport as well as very short solid-state diffusion lengths. This concept is compatible with many battery chemistries, and the short solid-state diffusion lengths provided by this system may even enable the use of new anode and cathode materials not previously considered acceptable due to their low ion and electrical conductivities. The bicontinuous conductive scaffold approach provides flexibility in electrode thickness, thickness of the electrolytically active phase and characteristic pore diameter, enabling optimization to match the characteristic kinetics of a given battery chemistry. The ultrafast rate performance demonstrated by the bicontinuous electrode provides an electrochemical storage technology with the power density of a supercapacitor and the energy density of a battery. Further optimization, through the design of matched cathodes, anodes, separator membranes and high-rate compatible electrolyte chemistries should yield additional improvements in charge and discharge kinetics. Finally, the fabrication process applied is compatible with large-volume manufacturing approaches, and thus has the potential to impact both small- and large-scale applications.

Methods

Macroporous nickel fabrication. Macroporous nickel was fabricated as described previously[30] with the following modifications. The fabricated colloidal crystal was annealed at 95 °C for 2 h before nickel electrodeposition. The etching solution containing ~0.5–1 M Ni^{2+} was prepared by electrochemically dissolving nickel metal into EP1250 (Technic Corp) at 6 V. The macroporous nickel was electropolished in this solution by 6 V pulses (80 ms on and 16 s off) at 60 °C.

NiOOH electrodeposition. An aqueous solution of 0.5 M $NiSO_4$, 0.5 M Na_2SO_4 and 0.5 M CH_3COONa was prepared. Anodic pulses (1.4 V; 1 s on, 4 s off, ~500 cycles) were applied to the macroporous nickel electrode using this solution and a platinum counter-electrode at 60 °C.

MnO_2 electrodeposition. An aqueous solution of 0.5 M $MnSO_4$ and 0.5 M CH_3COONa was prepared. About 10 wt% ethanol was added to improve the wetting of the macroporous nickel. Anodic pulses (0.7–1.5 V; 1 s on, 10 s off, ~300 cycles) were applied to the macroporous nickel electrode using this solution and a platinum counter-electrode at 35 °C.

MnO_2 lithiation. The MnO_2-coated electrode and a finely ground 3:2 mole ratio of $LiNO_3$ and LiOH were placed into an Al_2O_3 crucible and heated to 300 °C for ~0.5–2 h. After cooling to room temperature, the sample was rinsed with deionized water to remove the salt residue and dried at 70 °C for 10 h.

Characterization. All the samples were characterized using a Hitachi S-4800 scanning electron microscope. Transmission electron microscopy (TEM) images were taken using a JEOL 2010 LaB6 microscope. X-ray diffraction was collected in Philips X'pert MRD and Rigaku D-max systems. Electrochemical characterization of the NiOOH electrode was performed in an aqueous solution of 6 M KOH and 10 wt% LiOH. The lithium-ion battery was assembled with a commercial graphite anode, Celgard 2500 separator and non-aqueous electrolyte (1 M $LiClO_4$ into a 1:1 mass ratio mixture of ethylene carbonate and dimethylene carbonate) in an argon-filled glove box. Nickel oxyhydroxide was selectively dissolved in 0.1 M HCl solution with ultrasonication, and lithiated MnO_2 was dissolved in 3 M HNO_3 and 3 M HCl. The electrode nickel and manganese ion content was determined by inductively coupled plasma atomic emission spectroscopy (Optima 2000 DV, Perkin Elm).

Received 21 October 2010; accepted 24 February 2011; published online 20 March 2011

References

1. Taberna, L., Mitra, S., Poizot, P., Simon, P. & Tarascon, J. M. High rate capabilities Fe_3O_4-based Cu nano-architectured electrodes for lithium-ion battery applications. *Nature Mater.* **5,** 567–573 (2006).
2. Kang, B. & Ceder, G. Battery materials for ultrafast charging and discharging. *Nature* **458,** 190–193 (2009).
3. Chung, S. Y., Bloking, J. T. & Chiang, Y. M. Electronically conductive phospho-olivines as lithium storage electrodes. *Nature Mater.* **1,** 123–128 (2002).
4. Yao, M. *et al.* Nickel substrate having three-dimensional micronetwork structure for high-power nickel/metal-hydride battery. *Electrochem. Solid State Lett.* **10,** A56–A59 (2007).
5. Bruce, P. G., Scrosati, B. & Tarascon, J. M. Nanomaterials for rechargeable lithium batteries. *Angew. Chem. Int. Ed.* **47,** 2930–2946 (2008).
6. Kang, K. S., Meng, Y. S., Breger, J., Grey, C. P. & Ceder, G. Electrodes with high power and high capacity for rechargeable lithium batteries. *Science* **311,** 977–980 (2006).
7. Rolison, D. R. *et al.* Multifunctional 3D nanoarchitectures for energy storage and conversion. *Chem. Soc. Rev.* **38,** 226–252 (2009).
8. Arico, A. S., Bruce, P., Scrosati, B., Tarascon, J. M. & Van Schalkwijk, W. Nanostructured materials for advanced energy conversion and storage devices. *Nature Mater.* **4,** 366–377 (2005).
9. Wang, Y. G., Wang, Y. R., Hosono, E. J., Wang, K. X. & Zhou, H. S. The design of a $LiFePO_4$/carbon nanocomposite with a core–shell structure and its synthesis by an *in situ* polymerization restriction method. *Angew. Chem. Int. Ed.* **47,** 7461–7465 (2008).
10. Doherty, C. M., Caruso, R. A., Smarsly, B. M., Adelhelm, P. & Drummond, C. J. Hierarchically porous monolithic $LiFePO_4$/carbon composite electrode materials for high power lithium ion batteries. *Chem. Mater.* **21,** 5300–5306 (2009).
11. Cui, L. F., Yang, Y., Hsu, C. M. & Cui, Y. Carbon-silicon core-shell nanowires as high capacity electrode for lithium ion batteries. *Nano Lett.* **9,** 3370–3374 (2009).
12. Long, J. W., Dunn, B., Rolison, D. R. & White, H. S. Three-dimensional battery architectures. *Chem. Rev.* **104,** 4463–4492 (2004).
13. Whitehead, A. H. & Schreiber, M. Current collectors for positive electrodes of lithium-based batteries. *J. Electrochem. Soc.* **152,** A2105–A2113 (2005).

14. Yao, M., Okuno, K., Iwaki, T., Awazu, T. & Sakai, T. Long cycle-life $LiFePO_4$/Cu–Sn lithium ion battery using foam-type three-dimensional current collector. *J. Power Sources* **195,** 2077–2081 (2010).
15. Ripenbein, T., Golodnitsky, D., Nathan, M. & Peled, E. Electroless nickel current collector for 3D-microbatteries. *J. Appl. Electrochem.* **40,** 435–444 (2010).
16. Plichta, E. *et al.* A rechargeable Li/Li_xCoO_2 Cell. *J. Power Sources* **21,** 25–31 (1987).
17. Shembel, E. M. *et al.* Problems of corrosion and other electrochemical side processes in lithium chemical power sources with non-aqueous electrolytes. *J. Power Sources* **54,** 421–424 (1995).
18. Yao, M. *et al.* $LiFePO_4$-based electrode using micro-porous current collector for high power lithium ion battery. *J. Power Sources* **173,** 545–549 (2007).
19. Kim, J. H., Myung, S. T. & Sun, Y. K. Molten salt synthesis of $LiNi_{0.5}Mn_{1.5}O_4$ spinel for 5 V class cathode material of Li-ion secondary battery. *Electrochim. Acta* **49,** 219–227 (2004).
20. Guo, J. C. & Wang, C. S. A polymer scaffold binder structure for high capacity silicon anode of lithium-ion battery. *Chem. Commun.* **46,** 1428–1430 (2010).
21. Reddy, A. L. M., Shaijumon, M. M., Gowda, S. R. & Ajayan, P. M. Coaxial MnO_2/carbon nanotube array electrodes for high-performance lithium batteries. *Nano Lett.* **9,** 1002–1006 (2009).
22. Lee, S. W. *et al.* High-power lithium batteries from functionalized carbon-nanotube electrodes. *Nature Nanotech.* **5,** 531–537 (2010).
23. Fischer, A. E., Pettigrew, K. A., Rolison, D. R., Stroud, R. M. & Long, J. W. Incorporation of homogeneous, nanoscale MnO_2 within ultraporous carbon structures via self-limiting electroless deposition: implications for electrochemical capacitors. *Nano Lett.* **7,** 281–286 (2007).
24. Ergang, N. S. *et al.* Photonic crystal structures as a basis for a three-dimensionally interpenetrating electrochemical-cell system. *Adv. Mater.* **18,** 1750–1753 (2006).
25. Ergang, N. S., Fierke, M. A., Wang, Z., Smyrl, W. H. & Stein, A. Fabrication of a fully infiltrated three-dimensional solid-state interpenetrating electrochemical cell. *J. Electrochem. Soc.* **154,** A1135–A1139 (2007).
26. Wang, Z., Fierke, M. A. & Stein, A. Porous carbon/tin (IV) oxide monoliths as anodes for lithium-ion batteries. *J. Electrochem. Soc.* **155,** A658–A663 (2008).
27. Ergang, N. S., Lytle, J. C., Yan, H. W. & Stein, A. Effect of a macropore structure on cycling rates of $LiCoO_2$. *J. Electrochem. Soc.* **152,** A1989–A1995 (2005).
28. Sakamoto, J. S. & Dunn, B. Hierarchical battery electrodes based on inverted opal structures. *J. Mater. Chem.* **12,** 2859–2861 (2002).
29. Stephenson, D. E., Hartman, E. M., Harb, J. N. & Wheeler, D. R. Modeling of particle–particle interactions in porous cathodes for lithium-ion batteries. *J. Electrochem. Soc.* **154,** A1146–A1155 (2007).
30. Yu, X. D., Lee, Y. J., Furstenberg, R., White, J. O. & Braun, P. V. Filling fraction dependent properties of inverse opal metallic photonic crystals. *Adv. Mater.* **19,** 1689–1692 (2007).
31. Wu, M. S., Huang, Y. A. & Yang, C. H. Capacitive behavior of porous nickel oxide/hydroxide electrodes with interconnected nanoflakes synthesized by anodic electrodeposition. *J. Electrochem. Soc.* **155,** A798–A805 (2008).
32. Tench, D. & Warren, L. F. Electrodeposition of conducting transition-metal oxide hydroxide films from aqueous-solution. *J. Electrochem. Soc.* **130,** 869–872 (1983).
33. Motupally, S., Streinz, C. C. & Weidner, J. W. Proton diffusion in nickel hydroxide—prediction of active material utilization. *J. Electrochem. Soc.* **145,** 29–34 (1998).
34. Mao, Z., Devidts, P., White, R. E. & Newman, J. Theoretical analysis of the discharge performance of a $NiOOH/H_2$ cell. *J. Electrochem. Soc.* **141,** 54–63 (1994).
35. Corrigan, D. A. & Knight, S. L. Electrochemical and spectroscopic evidence on the participation of quadrivalent nickel in the nickel-hydroxide redox reaction. *J. Electrochem. Soc.* **136,** 613–619 (1989).
36. Reimers, J. N., Fuller, E. W., Rossen, E. & Dahn, J. R. Synthesis and electrochemical studies of $LiMnO_2$ prepared of low-temperatures. *J. Electrochem. Soc.* **140,** 3396–3401 (1993).

Acknowledgements

This work was supported by the US Department of Energy, Division of Materials Sciences (DE-FG02-07ER46471) through the Materials Research Laboratory at the University of Illinois at Urbana-Champaign (energy storage studies), and the US Army Research Laboratory and US Army Research Office (DAAD19-03-1-0227) (three-dimensional electrode fabrication).

Author contributions

H.Z., X.Y. and P.V.B. designed the experiments. H.Z and X.Y. performed and analysed the experiments. H.Z., X.Y. and P.V.B. wrote the manuscript. P.V.B. supervised the project.

Additional information

The authors declare no competing financial interests. Supplementary information accompanies this paper at www.nature.com/naturenanotechnology. Reprints and permission information is available online at http://npg.nature.com/reprintsandpermissions/. Correspondence and requests for materials should be addressed to P.V.B.